Surface reconstructions and relaxation effects in a centre-symmetrical crystal: the {00.1} form of calcite ($CaCO_3$)†

Marco Bruno,* Francesco Roberto Massaro, Mauro Prencipe and Dino Aquilano

Received 11th February 2010, Accepted 10th May 2010
DOI: 10.1039/c002969f

Reconstructing polar surfaces of crystals represents the pathway needed to obtain both surface stability and minimum of surface free energy. Knowing these equilibrium conditions is, in turn, necessary to interpret surface kinetics, especially when foreign adsorption or epitaxial phenomena are involved. Here we reconstructed the {00.1} dipolar surfaces of a centre-symmetrical crystal, calcite ($CaCO_3$), either by removing one half of the ions in the outermost layer of the face, or by applying calcite to the octopolar Lacmann's model, already proposed for NaCl-like lattices. This second way respects the bulk symmetry of the crystal and was carried out by removing $^3/_4$ of the ions in the outermost layer and ¼ in the second to last one, respectively. Relaxed and athermal surface energies were determined at the empirical level and the octopolar CO_3 terminated {00.1} form was the most stable. Moreover, calculation shows that the {00.1} form, along with the {10.4} and {01.2} rhombohedra, can enter the athermal equilibrium morphology of the calcite crystal. Finally, when recollecting our results on the reconstructed {01.2} form of calcite and {111} NaCl octahedron, it can be stressed that the bulk crystal symmetry has to be considered if one aims to achieve the self consistency of the surface reconstruction (Curie's principle).

1. Introduction

The real surface profile of a (*hkl*) face rarely coincides with the ideal *hkl* lattice plane. In other words, the *hkl* plane is geometrically abstracted from the crystal structure while, to generate the corresponding surface profile, one has to consider the face character: flat (F), stepped (S) or kinked (K), according to the Hartman–Perdok theory,[1] along with its interactions with the mother phase. Calculation shows that stability problems arise, owing to the surface polarity, either in polar crystals or on peculiar faces of non-polar crystals, since the infinite 2D array of iso-oriented surface dipole moments makes infinite the value of the electrical field in the surface sites. Dipolar surfaces (type-3 surfaces, according to Tasker's classification[2]) can belong to two classes of crystals: to the polar ones, such as ZnS–wurtzite like ($P6_3mc$) or ZnS–sphalerite like ($F\bar{4}3m$) lattices, and to those, non-polar, where the surface polarity ensues from the alternating layers of positive and negative charges parallel to a given crystal face (such as the {111} form of the NaCl–like fcc lattice).

In spite of their instability, these surfaces often exist both in nature and in the laboratory and, to explain their occurrence either at equilibrium or during growth, one has to invoke:

(i) surface modifications at the atomic level induced by adsorption of foreign substances (see Bruno *et al.*,[3] and references therein);

(ii) a reconstruction of the surfaces to cancel out the 2D-dipole arrays and/or

(iii) a rearrangement of the electronic structure resulting in an effective charge transfer between the polar surfaces, as it was suggested for some forms of covalent phases:[4,5]

In any case, a criterion for surface reconstruction or for its electronic rearrangement is needed, especially when dealing with foreign adsorption.

Reconstructions found in the literature usually consist in removing one half of the atoms from the outermost *hkl* layer and in relocating them on its centre-symmetrical $\overline{hkl}$ plane, regardless of the topology obtained from the atoms removal. Actually, this kind of reconstruction is not self-consistent even if both conditions of electroneutrality and dipole annihilation on the surface are fulfilled. In fact, there are many ways to remove one half of the surface ions and then to associate, to each of them, the related surface energy value. Unluckily, a serious drawback arises when dealing with the search for the minimum of the surface energy, $\gamma_{(hkl)}$, of the reconstructed surfaces.

In this paper we mainly deal with the reconstruction of the {00.1} form of calcite ($CaCO_3$, space group $R\bar{3}c$, hexagonal frame)[6] for two reasons:

(i) the high symmetry of this form represents an interesting case study to prove that the symmetry of the crystal bulk cannot be neglected when one aims at finding the surface profile of minimum energy.

(ii) calcite is a centre-symmetrical crystal exhibiting polar faces; further, it is not only the most celebrated crystal from the historical point of view but, owing to its complex and strongly anisotropic structure, is of more and more increasing importance in both inorganic and biological systems. As an example, the surface structure of the {00.1} and {01.2} forms of calcite seems to offer the most suitable interfaces for the preparation of different organic/inorganic monolayer systems in biomineralization processes.[7–14]

Dipartimento di Scienze Mineralogiche e Petrologiche, Università degli Studi di Torino, Via Valperga Caluso 35, I-10125 Torino, Italy. E-mail: marco.bruno@unito.it; Fax: +390116705128; Tel: +390116705131

† Electronic supplementary information (ESI) available: Tables SI–SIV. See DOI: 10.1039/c002969f

While {01.2} is a F form, the {00.1} is a K one. Their surfaces are made of alternating layers of Ca ions and CO_3 groups, as it comes out when the structure is observed along any direction perpendicular to the [001] triad axis. Consequently, the ideal {01.2} and {00.1} forms exhibit iso-oriented dipoles in their outermost layers and hence they have unstable terminations that need to be reconstructed.

Recently, Bruno *et al.*[15] succeeded in stabilizing the {01.2} form of calcite by considering two surface reconstructions coupled with two alternative terminations (either Ca or CO_3 ions), as originally proposed by Massaro *et al.*[16] The reconstructed surfaces were obtained by removing 50% of the ion rows in the outermost layer, in two different ways:

(i) in the first mode, the direction of the remaining rows was chosen arbitrarily, *i.e.* without constraints to a predefined criterion;

(ii) in the second one, the direction of the remaining rows respected the bulk symmetry due to the planes perpendicular to {01.2} faces.

Then, the corresponding surface energies at 0 K were calculated and the reconstructed face, CO_3 terminated and respecting the bulk symmetry, resulted in being the more stable.

An analogous problem was faced[3,17] in the case of the {111} form of NaCl (space group *Fm*3*m*), which consists of alternating layers of Na and Cl ions stacked along the <111> three-fold axes. As for the {01.2} form of calcite, two kinds of NaCl {111} reconstructions were considered:

(i) the first one (labelled R1, hereinafter) was carried out by modifying the sole outer plane of the slab.[17] Thus, one half of the <1 $\bar{1}$0> rows (either Na or Cl ions) was moved from the outmost plane of the {111} slab to a new plane at the bottom, with the aim at obtaining a slab which was rendered symmetrical with respect to a central ion plane.

(ii) the second reconstruction (R2) was obtained by removing 75% of the ions in the outer layer of the slab and 25% of the other ion species in the second to last one.[3] This way, named "octopolar reconstruction", was firstly proposed by Hartman[18] and later on by Lacmann[19] who imagined the NaCl-like structures as built by a 3D array of octopoles which consist of cubes (each containing four NaCl units), electrically neutral and lacking a dipole moment.

Both R1 and R2 reconstructions generated a neutral and non polar slab, but only the octopolar one saved the three-fold symmetry intrinsic to the {111} form. Further, calculation showed that the relaxed surface energies of the $\{111\}_{R1}$ form were sensibly higher than those belonging to $\{111\}_{R2}$.

On the ground of these preliminary results, we aim at investigating the stability of the {00.1} form of calcite, which shows the same polarity problem of the {111} NaCl surfaces, by keeping in mind that fulfilling the electro-neutrality of the infinite {00.1} slab, along with the vanishing of its total dipole moment, are only necessary conditions for the convergence of its surface energy to an asymptotic and finite value. Actually, such conditions are not sufficient to solve the problem, since the boundary conditions, related to the symmetry of the surface we are dealing with, cannot be neglected.

The structure of calcite, when viewed perpendicularly to its three-fold [001] and non polar axis, is very similar to that of rock-salt projected perpendicularly to the <111> directions (Fig. 1).

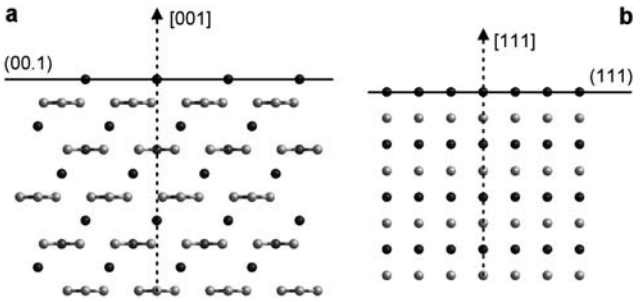

Fig. 1 (a) Calcite and (b) NaCl-like unrelaxed structures viewed perpendicularly to the three-fold [001] and <111> axis, respectively. Owing to the alternating and equidistant layers of opposite charges, the electrical field at the surface of infinite crystal slabs becomes infinite.

Indeed, it can be simply imagined as a replacement of the Na cations by Ca and of the Cl anions by CO_3 groups, coupled with a compression along the [001] axis. Hence, both R1 and R2 reconstructions already employed for the {111} NaCl surface, can also be considered for stabilizing the {00.1} surface of calcite. Moreover, both reconstructions being either Ca or CO_3 terminated, we will use the notation $(00.1)^{B}_{A}$, where A = R1 or R2, and B = Ca or CO_3, to distinguish among the different surface reconstructions and terminations.

Finally, in order to determine which one of the reconstructions is favoured, the surface energies related to the four $(00.1)^{Ca}_{R1}$, $(00.1)^{CO_3}{}_{R1}$, $(00.1)^{Ca}_{R2}$ and $(00.1)^{CO_3}{}_{R2}$ profiles were calculated, before and after surface relaxation.

2. Computational details

Calculations (optimizations of slab geometries and surface energy estimates) were performed by using the inter-atomic potential for calcite developed by Rohl *et al.*[20] (Rohl potential hereinafter) and the General Utility Lattice Program (GULP) simulation code[21] which, being based on force field methods, allows the calculation of structures and properties of minerals from a given set of empirical potentials. The parameters of the Rohl potential were obtained by fitting structural data for both calcite and aragonite, as well as physical properties (elastic and dielectric constants) and phonon frequencies.[20] Moreover, this potential reproduced very successfully the equilibrium geometries and the surface energy values of the {01.2} faces obtained from *ab initio* calculations at DFT (Density Functional Theory; B3LYP Hamiltonian[22]) level,[15] as well as the experimental observations of the surface relaxation of the {10.4} form.[20] Geometry optimization is considered converged when the gradient tolerance and the function tolerance (*gtol* and *ftol* adimensional parameters in GULP) are smaller than 0.0001 and 0.00001, respectively.

To further test the performance and reliability of such an empirical potential, we determined the equilibrium geometry and the surface energy of the (10.4) face of calcite, at DFT level, and we compared the results with the previous ones obtained by means of the Rohl potential. Geometry optimizations of the (10.4) slabs were obtained by means of the *ab initio* CRYSTAL06 code,[23] which implements the Hartree–Fock and Kohn–Sham self consistent field (SCF) method for the study of periodic

systems.[24] The calculations were performed at DFT level; the B3LYP Hamiltonian[22] was used, which contains a hybrid Hartree–Fock/Density-Functional exchange–correlation term. Details on the computational parameters are reported in Bruno *et al.*[15]

2.1. Slab geometry optimization

The (00.1) and (10.4) surfaces were studied by using the 2D-slab model.[25] (00.1) and (10.4) slabs of varying thickness were generated by separating the bulk structure along the plane of interest, and by eliminating the atoms in excess, in order to achieve the R1 and R2 reconstructions. The reconstruction of the (00.1) face was obtained by using a (2 × 2) cell in the 00.1 plane, while the calculations on the (10.4) face were performed by considering the original (1 × 1) cell.

At the empirical level (GULP program), the geometry optimization was performed by considering the slab subdivided into two regions: region 1, which contains both the surface and the underlying atomic layers that are allowed to relax, and region 2 which has the same number of layers of region 1, and contains the rest of the slab material where no relaxation with respect to the bulk crystal structure is assumed to occur.

At the *ab initio* DFT level (CRYSTAL06 program) the geometry optimization was performed by considering the reconstructed slab limited by two centre-symmetry related surfaces, and allowing the relaxation of the positions of all of the atoms.

The slab geometry was optimized starting from the values calculated at the DFT level by Prencipe *et al.*[26] With the GULP program, the geometry optimization was performed by means of the Newton–Raphson method, whereas in CRYSTAL06 the geometry optimization is performed by means of a modified conjugate gradient algorithm.[27]

At the empirical level, the geometry optimization (atomic coordinates) was performed for both R1 and R2 (00.1) slabs; the calculations were done by considering slabs with thickness up to ten layers (in both the regions 1 and 2), which are sufficient to reproduce bulk-like properties at the centre of the slab and to obtain a careful description of the surface. Concerning the DFT level, the geometry optimizations (lattice parameters and atomic coordinates) were performed for the (10.4) slabs; in this case, a six layers slab was sufficient to reproduce bulk-like properties at the slab centre. Tables listing lattice parameters and atomic coordinates of the optimized slabs are available as ESI.†

2.2. Calculation of the surface energy

According to the standard two-regions strategy employed by GULP, the specific surface energy (γ, J m^{-2}) was evaluated from the energy of the surface block (U_s, region 1) and the energy of a portion of bulk crystal (U_b) containing the same number of atoms as the surface block. Both energies have been referred to A, the common surface area of the primitive unit cell:[28]

$$\gamma = \frac{U_s - U_b}{A}$$

A ten layers slab (in both the regions 1 and 2) was sufficient to reach convergence on the $\gamma_{(00.1)}$ values.

According to the CRYSTAL06 strategy, γ has been calculated by means of the relation:[25]

$$\gamma = \lim_{n\to\infty} E_s(n) = \lim_{n\to\infty} \frac{E(n) - n[E(n) - E(n-1)]}{2A}$$

where n is the number of layers in the slab and $E(n)$ is the energy of a n-layer slab; the factor 2 accounts for the upper and lower surfaces of the slab. $E_s(n)$ is thus the specific energy required to form the surface from the bulk. As more layers are added in the calculation ($n \rightarrow \infty$), $E_s(n)$ will converge to the specific surface energy; a 6-layer slab was sufficient to reach convergence on the $\gamma_{(10.4)}$ value.

2.3. (10.4) surface structure and energy: comparison between empirical and *ab initio* calculations

The equilibrium geometry of the (10.4) slab obtained at DFT level is reported in Fig.2.

In agreement with the calculations performed with the Rohl potential, a very slight relaxation of the surface is observed, the (10.4) face being a very compact one. Moreover, $\gamma_{(10.4)}$ = 0.503 J m^{-2}, the relaxed value calculated with the B3LYP Hamiltonian (Table 1), closely agrees with that of 0.534 J m^{-2}, obtained by Rohl *et al.*,[20] who studied the (10.4) slab by using both the (1 × 1) and the (2 × 1) cells. In this work, only the (1 × 1) cell has been considered, since the *ab initio* calculations are very expensive from a computational point of view. It should also be noted that previous *ab initio* DFT calculations[29,30] performed with the PBE GGA functional[31] gave γ values which were significantly lower: 0.380–0.420 J m^{-2} (Table 1).

Considering the empirical level, a wide range of relaxed $\gamma_{(10.4)}$ values can be found in the literature, according to the specific inter-atomic potentials employed by each author. As a matter of fact, the calcite force field developed by Pavese *et al.*[32] provides an estimate of the relaxed $\gamma_{(10.4)}$ value which is higher by ~10–12% (0.590–0.600 J m^{-2}) than that found by Rohl *et al.*[20] (Table 1). Conversely, the energies calculated by Parker *et al.*[33] and by Hwang *et al.*[34] were 0.230 and 0.860 J m^{-2}, respectively.

Since the (10.4) and (01.2) equilibrium geometries, and both the $\gamma_{(10.4)}$ and $\gamma_{(01.2)}$ values obtained at B3LYP level, as well as the experimental observations of the surface relaxation of the (10.4) face,[20] are successfully reproduced by the Rohl potential, we consider the latter to be reliable enough to reproduce the surface geometry and energy of the reconstructed (00.1) face;

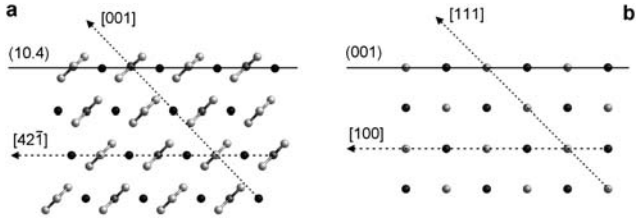

Fig. 2 (a) [010] projection of the relaxed structure of the (10.4) calcite slab, resulting from the optimization at B3LYP level (see text for details). (b) [010] projection of the relaxed structure of the (001) NaCl slab. The comparison evidences that the slab planes are electrically neutral and scarcely affected by the relaxation, for both structures.

Table 1 Relaxed (γ^r) and unrelaxed (γ^u) surface energies at 0 K of the {10.4} form of calcite

Authors	γ^r/J m^{-2}	γ^u/J m^{-2}	Potential/Hamiltonian
This work	0.503	0.567	B3LYP[22]
Parker *et al.*[29]	0.420		PBE GGA[31]
Kerisit *et al.*[30]	0.380–0.420		
Parker *et al.*[33]	0.230		Parker *et al.*[33]
Parker *et al.*[29]	0.590		Pavese *et al.*[32]
Titiloye *et al.*[36]	0.590		
de Leeuw and Parker[35]	0.600		
de Leeuw and Parker[37]	0.590		
Hwang *et al.*[34]	0.860	0.930	Hwang *et al.*[34]
Rohl *et al.*[20]	0.534	0.707[a]	Rohl *et al.*[20]

[a] Value not reported by Rohl *et al.*,[20] but calculated in this work by using their potential.

a detailed discussion of the (01.2) equilibrium geometries obtained both at *ab initio* and empirical level, is reported in a previous paper by Bruno *et al.*[15] The other different inter-atomic potentials are indeed able to reproduce the bulk properties, but they seem to be less effective when dealing with lower coordination environments (surfaces). In particular, this should be true for the potentials developed by Parker *et al.*[33] and Hwang *et al.*,[34] who provide $\gamma_{(10.4)}$ values which are very different with respect to those determined in this work at B3LYP level, and by Parker *et al.*[29] and Kerisit *et al.*,[30] at the PBE GGA level.

3. Results and discussion

3.1. R1 reconstruction and relaxation: the $(00.1)^{Ca}_{R1}$ and $(00.1)^{CO_3}_{R1}$ surface structures

$(00.1)^{Ca}_{R1}$ and $(00.1)^{CO_3}_{R1}$ slabs were reconstructed by removing 50% of Ca and CO_3 ions in the outermost layer, respectively. Their equilibrium geometries, obtained with the force field method, are reported in Fig. 3.

Hereinafter, to describe the (00.1) slab structure, the term *slice* will be used to indicate a fraction of slab made up by two adjacent layers of Ca and CO_3 ions: the slice corresponds to a $d_{00.6}$ thickness, as allowed by the systematic extinction rules. Since a detailed discussion of the surface structure (*e.g.*, angles and inter-atomic distances) is beyond the scope of this work, tables listing lattice parameters and atomic coordinates of the optimized slabs are available as ESI.†

The first slice of the $(00.1)^{Ca}_{R1}$ slab shows a higher distortion with respect to either the underneath ones or the bulk geometry; namely, the CO_3 groups are rotated about both the [010] axis and the [001] direction. Furthermore, the first slice is more compact with respect to the underlying ones, since the Ca ions and the centres of mass of the CO_3 groups tend to dispose on a common plane. However, the relaxation mainly concerns the five uppermost slices of the slab. The $(00.1)^{CO_3}_{R1}$ slab exhibits a lower relaxation than that of the just mentioned one, the four uppermost slices only being affected by a sensible rearrangement. Further, as in the previous case, the CO_3 groups are rotated about both the [010] axis and about the [001] direction. It is also worth noting that the strongest rotation of the CO_3 ions is localized in the second slice of the slab.

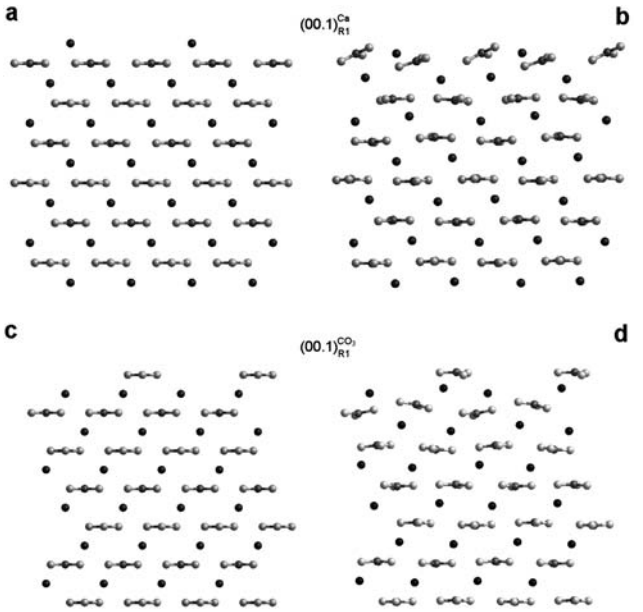

Fig. 3 [010] projection of the: (a) unrelaxed and (b) relaxed structure of the $(00.1)^{Ca}_{R1}$ slab; (c) unrelaxed and (d) relaxed structure of the $(00.1)^{CO_3}_{R1}$ slab. Relaxed structures result from the optimization at empirical level (see text for details).

3.2. R2 octopolar reconstruction and relaxation: the $(00.1)^{Ca}_{R2}$ and $(00.1)^{CO_3}_{R2}$ surface structures

The $(00.1)^{Ca}_{R2}$ and $(00.1)^{CO_3}_{R2}$ slabs were reconstructed by removing 75% of the ions in the outer layer and 25% of the ions in the underlying one; the unrelaxed octopolar $(00.1)^{Ca}_{R2}$ face is drawn in Fig. 4 where one can see that this reconstruction preserves the three-fold symmetry axis.

The optimized geometries of the $(00.1)^{Ca}_{R2}$ and $(00.1)^{CO_3}_{R2}$ slabs are reported in Fig. 5. In both cases the CO_3 groups are rotated about both the [100] and the [001] direction, and the relaxation mainly concerns the four uppermost slices of the slab.

3.3. Surface energies of $(00.1)^{Ca}_{R1}$, $(00.1)^{CO_3}_{R1}$, $(00.1)^{Ca}_{R2}$ and $(00.1)^{CO_3}_{R2}$ faces at 0 K

From Table 2 it follows that the stability order of the relaxed faces is $(00.1)^{CO_3}_{R2} < (00.1)^{CO_3}_{R1} < (00.1)^{Ca}_{R1} < (00.1)^{Ca}_{R2}$ whereas, for

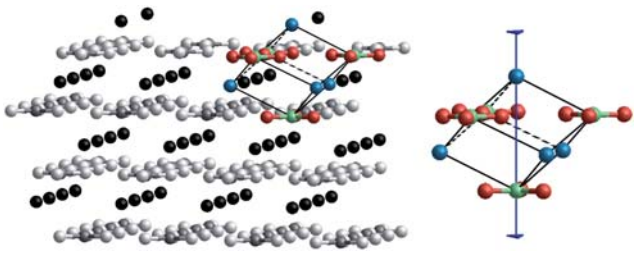

Fig. 4 Octopolar reconstruction of the Ca terminated (00.1) face of calcite, obtained by removing 75% of the Ca ions in the outer layer and 25% of the CO_3 groups in the underneath one. The calcite octopole, composed by four Ca ions and four CO_3 groups stacked along the three-fold axis, reproduces the {10.4} cleavage rhombohedron.

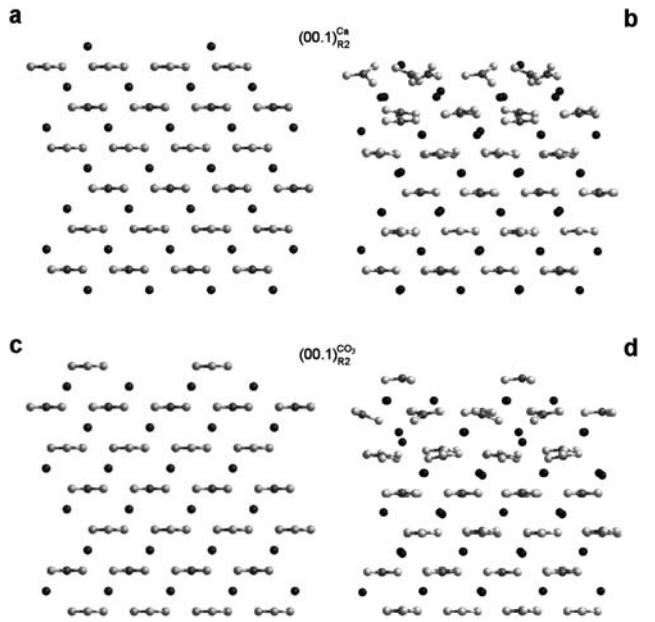

Fig. 5 [010] projection of the: (a) unrelaxed and (b) relaxed structure of the $(00.1)^{Ca}_{R2}$ slab; (c) unrelaxed and (d) relaxed structure of the $(00.1)^{CO3}_{R2}$ slab. Relaxed structures result from the optimization at the empirical level (see text for details).

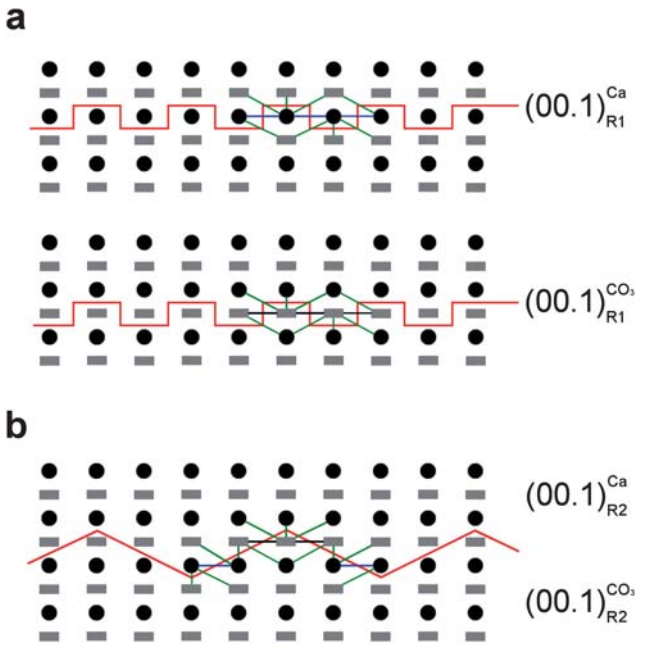

Fig. 6 Schematic drawing of the (a) R1 and (b) R2 reconstructions of the (00.1) polar face. The Ca and CO_3 ions are represented by black circles and grey rectangles, respectively. The red line identifies the reconstructed surfaces, which are generated by dividing the crystal along the 00.1 plane. The Ca–CO_3, Ca–Ca and CO_3–CO_3 interactions are represented by green, blue and black lines, respectively.

the unrelaxed ones, $(00.1)^{CO_3}{}_{R2} = (00.1)^{Ca}_{R2} < (00.1)^{CO_3}{}_{R1} < (00.1)^{Ca}_{R1}$. The unrelaxed surface energies of the octopolar reconstructed faces are necessarily equal. This can be explained by considering that the two octopolar reconstructed surfaces (either Ca or CO_3 terminated) are each other complementary, at variance with the R1 reconstruction, and then the separation work needed to generate both of them must be the same, as follows from Fig. 6.

By only considering the first nearest neighbours, one can see that one has to break eight Ca–CO_3 and three Ca–Ca interactions to generate the $(00.1)^{Ca}_{R1}$ surface, whereas eight Ca–CO_3 and three CO_3–CO_3 interactions should be cut to obtain the $(00.1)^{CO_3}{}_{R1}$ surface (Fig. 6a). Then, the different values of the unrelaxed surface energies of the $(00.1)^{Ca}_{R1}$ and $(00.1)^{CO_3}{}_{R1}$ profiles are due to the deep differences between the Ca–Ca and CO_3–CO_3 interactions. Instead, two Ca–Ca, two CO_3–CO_3 and twelve Ca–CO_3 couples have to be broken to obtain both the $(00.1)^{Ca}_{R2}$ and $(00.1)^{CO_3}{}_{R2}$ surfaces (Fig. 6b). This implies equivalence of the $(00.1)^{Ca}_{R2}$ and $(00.1)^{CO_3}{}_{R2}$ unrelaxed surface energies.

Table 2 Unrelaxed and relaxed surface energies at 0 K of the {00.1} form of calcite

Authors	Face	γ^r/J m^{-2}	γ^u/J m^{-2}	Potential/ Hamiltonian
This work	$(00.1)^{Ca}_{R1}$	0.834	2.476	Rohl *et al.*[20]
	$(00.1)^{CO_3}{}_{R1}$	0.764	1.720	
	$(00.1)^{Ca}_{R2}$	0.849	1.654	
	$(00.1)^{CO_3}{}_{R2}$	0.711	1.654	
Parker *et al.*[33]	$(00.1)^{Ca}_{R1}$	1.600		Parker *et al.*[33]
de Leeuw	$(00.1)^{Ca}_{R1}$	0.970	2.580	Pavese *et al.*[32]
and Parker[35]	$(00.1)^{CO_3}{}_{R1}$	0.990		
de Leeuw	$(00.1)^{Ca}_{R1}$		2.620	
and Parker[37]	$(00.1)^{CO_3}{}_{R1}$		1.840	
Hwang *et al.*[34]	$(00.1)_{R1}$	1.440–1.450[a]	2.680–2.690[a]	Hwang *et al.*[34]
Parker *et al.*[29]	$(00.1)^{Ca}_{R1}$	0.660		PBE GGA[31]
	$(00.1)^{CO_3}{}_{R1}$	0.680		

[a] Values averaged over the two Ca and CO_3 terminated surfaces.

We can now show that the Rohl potential does not yield realistic unrelaxed γ values. As a matter of fact, there is a high discrepancy between the unrelaxed $\gamma_{(10.4)}$ and $\gamma_{(01.2)}$ values calculated at B3LYP level and those determined by using the Rohl potential. The unrelaxed $\gamma_{(10.4)}$ value reaches 0.567 and 0.707 J m^{-2} at B3LYP level and empirical level, respectively (Table 1). In the case of the (01.2) face,[15] at B3LYP level the unrelaxed $\gamma_{(01.2)}$ is 2.050 J m^{-2}, whereas at the empirical level $\gamma_{(01.2)}$ reaches 2.719 J m^{-2}. Indeed, at variance with the empirical calculations employing fixed model potentials, at the *ab initio* DFT (B3LYP) level an electronic relaxation is allowed. Charge relaxation is then exploited at B3LYP level to reduce the energy of the geometrical unrelaxed surface. In other words, when a quantum mechanical simulation is performed, the distribution of the electrons in the outermost layers of the slab is modified even when the atomic positions are not permitted to relax (unrelaxed geometry). As a consequence, since the force field cannot take into account the electronic relaxation, the values of the unrelaxed surface energy determined at the empirical level are always higher than those obtained at the *ab initio* level. This implies that also the relaxation energies ($\Delta E_{relax} = \gamma^{unrelaxed} - \gamma^{relaxed}$) calculated at the empirical level are physically ungrounded for a carbonate. For this reason we will not discuss further the unrelaxed surface energies of such faces.

No previous estimates of both relaxed and unrelaxed surface energies of the octopolar reconstructed {00.1} faces of calcite exist: in fact, in all of the previous work,[29,33,35–38] the R1

reconstruction only was considered in order to stabilize the (00.1) surface of calcite. Calculations on the R1 reconstructed faces were performed at the empirical level by de Leeuw and Parker[35,37] (see also Parker *et al.*[29] and Titiloye *et al.*[36]), by using the inter-atomic potential developed by Pavese *et al.*[32] They obtained $\gamma_{(00.1)} = 0.990$ and 0.970 J m^{-2} for relaxed $(00.1)^{CO_3}_{R1}$ and $(00.1)^{Ca}_{R1}$ faces (Table 2), respectively. These values are higher by ~30% and ~16%, respectively, than our estimates obtained with the inter-atomic Rohl potential. Such differences are in agreement with the previous calculations we carried out[15] on the reconstructed {01.2} form of calcite. Indeed, we calculated the relaxed surface energies of this reconstructed form by means of the inter-atomic Rohl potential and showed that these values do perfectly agree with those obtained at DFT level (by using the B3LYP Hamiltonian), but are significantly lower than those determined through the inter-atomic potential by Pavese *et al.*[32] Moreover, as mentioned above, the relaxed $\gamma_{(10.4)}$ value calculated by Rohl *et al.*[20] with their potential is lower by 11% than that calculated by using the Pavese *et al.*[32] potential.[29,35–37] Empirical calculations on the (00.1) slabs were also performed by Parker *et al.*[33] and Hwang *et al.*,[34] who obtained very high relaxed γ values (about twice our values). Then, once again, one can conclude that their potentials are not too effective to treat the surfaces of calcite crystals.

The R1 reconstruction was also investigated at the DFT level (PBE GGA functional) by Parker *et al.*[29] They obtained relaxed γ values (0.660 and 0.680 J m^{-2} for the $(00.1)^{Ca}_{R1}$ and $(00.1)^{CO_3}_{R1}$ faces, respectively) which are lower than those reported in this work.

From our calculations, the octopolar $(00.1)^{CO_3}_{R2}$ surface represents the more stable profile. This result, along with those obtained on the {01.2} form of calcite[15] and on the {111} form of NaCl,[3,17] seems to indicate the necessity to take into account the symmetry of the bulk crystal, which cannot be arbitrarily interrupted at the crystal surface, when a surface reconstruction is performed.

In order to verify the stability of the reconstructed surface geometries, the surface phonon dispersion across the Brillouin zone was determined in all directions for the optimized $(00.1)^{Ca}_{R1}$, $(00.1)^{CO_3}_{R1}$, $(00.1)^{Ca}_{R2}$ and $(00.1)^{CO_3}_{R2}$ slabs. For the (2 × 2) cell, no imaginary phonon modes were determined anywhere within the Brillouin zone: accordingly, both reconstructions seem to be allowed.

3.4. The equilibrium shape of calcite at 0 K

The equilibrium shape at 0 K of the calcite crystal is drawn in Fig. 7, having applied the Gibbs–Wulff's theorem[39] and considered the relaxed values calculated[15,20] through the Rohl potential, $\gamma_{(10.4)} = 0.534$, $\gamma_{(01.2)} = 0.750$ and $\gamma_{(00.1)^{CO_3}_{R2}} = 0.711$ J m^{-2}, where $\gamma_{(01.2)}$ is related to the CO_3 terminated surface which we reconstructed respecting the bulk symmetry.

Surprisingly, the {01.2} and {00.1} forms can enter the athermal equilibrium shape of calcite, at variance with all the previous works[29,33–37] where the {10.4} form is found to be the only one belonging to the equilibrium morphology.

It is worth emphasizing that we are here considering dry surfaces and, therefore, it is not sensible to compare our results, obtained for the athermal equilibrium, with the observations on

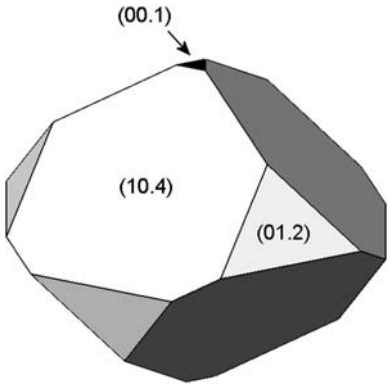

Fig. 7 The equilibrium shape of calcite at 0 K, obtained from the $\gamma_{(hk.l)}$ values (relaxed).

natural or laboratory crystals grown from aqueous solution. In order to correctly evaluate the equilibrium shape of crystals in an aqueous solution, it is fundamental to determine the effect of the adsorption of water molecules and/or impurities on the different surfaces. This can be done by performing molecular dynamic simulations (MD) of the calcite surfaces/solution interface, at the temperature of interest [see, for example, Spagnoli *et al.*[40] for an interesting MD study on the (10.4) face]. Duffy and Harding[38] performed MD calculations to study the (00.1) crystal/water interface at 300 K, considering a non specified R1 reconstruction and using the inter-atomic potentials by Pavese *et al.*;[32] according to their calculations, the {00.1} form cannot enter the equilibrium shape of calcite in solution. However, to give a further contribution to such an intriguing problem, it would be interesting to perform MD simulations of the (00.1) crystal/water interface starting from the octopolar model and using the Rohl potential.

3.5. Considering the surface symmetry

The octopolar reconstruction, when compatible with a given face, is unique and can be performed only in the way originally described by Hartman[18] and, successively, by Lacmann.[19] On the contrary, when the R1 reconstruction applies, there are several ways to cancel out the dipole moment by moving the charges in the outer layer, besides the one we mentioned above. As an example, the R1 way can be obtained:

(i) by joining two (or more) CO_3 (Ca) rows and leaving, consequently, two (or more) missing rows in between the successive steps (Fig. 8a), or

(ii) by disposing the ions (CO_3 or Ca) in such a way to obtain a chequered distribution (Fig. 8b).

To test the effect on the energy of two such latter R1 topologies, we performed the calculations on the reconstructed (00.1) slabs as represented in Fig. 8 and found that the relaxed γ values are 0.823 and 0.901 J m^{-2}, respectively, which are significantly higher than that related to the $(00.1)^{CO_3}_{R1}$ face, 0.764 J m^{-2}. We only considered the CO_3 terminated slabs because the relaxed γ value of the $(00.1)^{CO3}_{R1}$ face is lower than that of the $(00.1)^{Ca}_{R1}$ face (Table 2); the equilibrium geometries of the relaxed slabs are not discussed here (the output files generated by the GULP program are available on request).

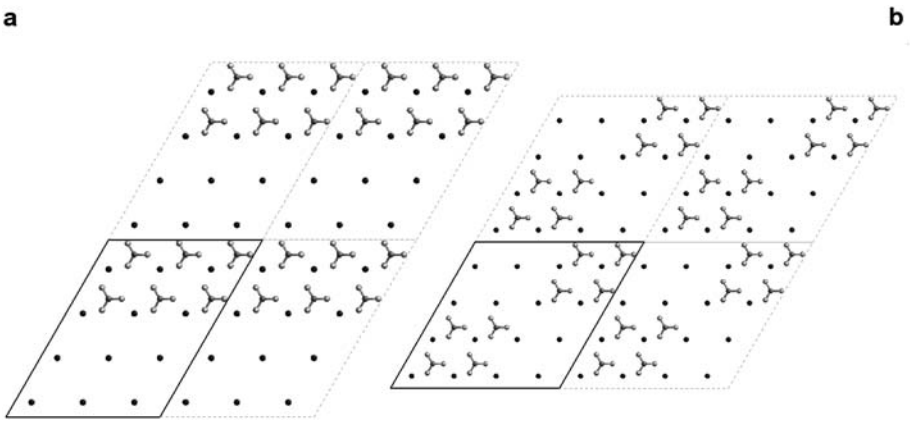

Fig. 8 [001] projection of the unrelaxed and reconstructed CO_3 terminated {00.1} faces. (a) The (00.1) face is reconstructed by removing two by two the rows of CO_3 ions in the outermost layer. (b) The (00.1) face is reconstructed by removing the CO_3 ions in the outermost layer in such a way as to obtain a chequered ion distribution. After each reconstruction 50% of the CO_3 ions was removed from the outermost layer.

These calculations outline once more the necessity to take into account the bulk symmetry of the crystal when a surface reconstruction is performed. We justify such necessity by considering that, at the equilibrium, an initially adsorbed population of atoms randomly distributed on a face rearranges itself in such a way as to minimize the surface energy. Then, it is quite reasonable to suppose that the crystal field symmetry forces the atoms to choose those sites on the surface which respect the symmetry imposed by the bulk. Concerning the octopolar model, it is worth recalling that it was born to predict the equilibrium shape and the surface energy of NaCl-like crystals and that it intrinsically respects the character of the faces (flat for {100}, stepped for {110} and kinked for {111} forms, respectively). Accordingly, the octopolar model is not a reconstruction *sensu stricto*, but is a way to foresee the most reasonable surface profile of a face for this kind of crystal lattice. This is the reason why the so-called "octopolar reconstruction" is favoured with respect to all the other ones when dealing with a face ruled by a three-fold symmetry. We can also express these considerations by means of the Curie's symmetry principle,[41] which may be formulated for the crystal surfaces as follows: the symmetry group of a crystal face in its mother phase is given by the maximal common subgroup of the symmetry group of the bulk crystal and of the symmetry group of the mother phase. For the crystal/vacuum system, only the symmetry group of the crystal bulk can impose constraints on the symmetry group of the face. Accordingly, the face should have the maximal subgroup of the symmetry of the crystal bulk projected along the normal to the surface.

4. Conclusion

In this paper, two different reconstructions of the {00.1} form of calcite were studied:

—the R1 reconstruction was performed by moving from the outer plane one half of ion rows (Ca or CO_3) to a new plane at the bottom to produce a slab that is symmetrical about a central plane;

—the R2 reconstruction (octopolar), by removing 75% of the ions in the outer layer of the slab and 25% in the underneath one. The results we obtained can be summarized as follows:

(i) Among all the reconstructed surfaces the most stable one was $(00.1)^{CO_3}{}_{R2}$, with a surface energy of 0.711 J m^{-2}. The octopolar reconstruction is favoured with respect to all the other ones when dealing with a face ruled by a three-fold symmetry since, according to Curie's principle, the symmetry group of a reconstructed surface must be a subgroup of the symmetry of the bulk crystal viewed along the normal to the surface.

(ii) The octopolar reconstructed and CO_3 terminated {00.1} form can enter the athermal equilibrium morphology of the calcite crystal.

(iii) When recollecting our previous results obtained on reconstructed {01.2} form of calcite and {111} NaCl octahedron, we can state that the bulk crystal symmetry has to be necessarily considered to achieve the self consistency of the surface reconstruction (Curie's principle).

(iv) Determining the most probable surface symmetry is of fundamental importance to gain more insights on twinning, impurities adsorption and epitaxy. Indeed, the modelization and interpretation of such phenomena require the knowledge of the structure of the interface on which the phenomenon occurs.

Acknowledgements

The authors acknowledge two anonymous referees for helpful comments.

References

1 P. Hartman and W. G. Perdok, *Acta Crystallogr.*, 1955, **8**, 49–52; P. Hartman and W. G. Perdok, *Acta Crystallogr.*, 1955, **8**, 521–524; P. Hartman and W. G. Perdok, *Acta Crystallogr.*, 1955, **8**, 525–529.
2 P. W. Tasker, *J. Phys. C: Solid State Phys.*, 1979, **12**, 4977–4984.
3 M. Bruno, D. Aquilano, L. Pastero and M. Prencipe, *Cryst. Growth Des.*, 2008, **8**, 2163–2170.
4 A. Pojani, F. Finocchi and C. Noguera, *Appl. Surf. Sci.*, 1999, **142**, 177–181.
5 A. Wander, F. Schedin, P. Steadman, A. Norris, R. McGrath, T. S. Turner, G. Thornton and N. M. Harrison, *Phys. Rev. Lett.*, 2001, **86**, 3811–3814.
6 E. N. Maslen, V. A. Streltsov and N. R. Streltsova, *Acta Crystallogr., Sect. B: Struct. Sci.*, 1993, **49**, 636–641.
7 J. Aizenberg, A. J. Black and G. M. Whitesides, *Nature*, 1999, **398**, 495–498.

8 A. M. Travaille, J. J. J. M. Donners, J. W. Gerritsen, N. A. J. M. Sommerdijk, R. J. M. Nolte and H. van Kempen, *Adv. Mater.*, 2002, **14**, 492–495.
9 S. Champ, J. A. Dickinson, P. S. Fallon, B. R. Heywood and M. Mascal, *Angew. Chem.*, 2000, **112**, 2828–2831.
10 S. Champ, J. A. Dickinson, P. S. Fallon, B. R. Heywood and M. Mascal, *Angew. Chem., Int. Ed.*, 2000, **39**, 2716–2719.
11 D. Volkmer, M. Fricke, C. Agena and J. Mattay, *J. Mater. Chem.*, 2004, **14**, 2249–2259.
12 J. Aizenberg, A. J. Black and G. M. Whitesides, *J. Am. Chem. Soc.*, 1999, **121**, 4500–4509.
13 D. D. Archibald, S. B. Qadri and B. P. Gaber, *Langmuir*, 1996, **12**, 538–546.
14 A. Barman, D. J. Ahn, A. Lio, M. Salmeron, A. Reichert and D. Charych, *Science*, 1995, **269**, 515–518.
15 M. Bruno, F. R. Massaro and M. Prencipe, *Surf. Sci.*, 2008, **602**, 2774–2782.
16 F. R. Massaro, L. Pastero, M. Rubbo and D. Aquilano, *J. Cryst. Growth*, 2008, **310**, 706–715.
17 M. Bruno, D. Aquilano and M. Prencipe, *Cryst. Growth Des.*, 2009, **9**, 1912–1916.
18 P. Hartman, *Bull. Soc. franç. Minér. Crist.*, 1959, **LXXXII**, 158–163.
19 R. Lacmann, in *Adsorption et Croissance Cristalline*, Coll. Intern. CNRS no. 152, 1965, p. 195.
20 A. L. Rohl, K. Wright and J. D. Gale, *Am. Miner.*, 2003, **88**, 921–925.
21 J. D. Gale, *J. Chem. Soc., Faraday Trans.*, 1997, **93**, 629–637.
22 A. D. Becke, *J. Chem. Phys.*, 1993, **98**, 5648–5652.
23 R. Dovesi, V. R. Saunders, C. Roetti, R. Orlando, C. M. Zicovich-Wilson, F. Pascale, B. Civalleri, K. Doll, N. M. Harrison, I. J. Bush, Ph. D'Arco and M. Llunell, *CRYSTAL06 User's Manual*, University of Torino, Torino, 2006.
24 C. Pisani, R. Dovesi and C. Roetti, *Hartree–Fock ab initio treatment of crystalline systems, Lecture Notes in Chemistry*, Springer, Berlin, Heidelberg, New York, 1988.
25 R. Dovesi, B. Civalleri, R. Orlando, C. Roetti and V. R. Saunders, in *Reviews in Computational Chemistry*, ed. B. K. Lipkowitz, R. Larter and T. R. Cundari, John Wiley and Sons Inc., New York, 2005, vol. 21, ch. 1, pp. 1–125.
26 M. Prencipe, F. Pascale, C. M. Zicovich-Wilson, V. R. Saunders, R. Orlando and R. Dovesi, *Phys. Chem. Miner.*, 2004, **31**, 559–564.
27 B. Civalleri, Ph. D'Arco, R. Orlando, V. R. Saunders and R. Dovesi, *Chem. Phys. Lett.*, 2001, **348**, 131–138.
28 D. H. Gay and A. L. Rohl, *J. Chem. Soc., Faraday Trans.*, 1995, **91**, 925–936.
29 S. C. Parker, S. Kerisit, A. Marmier, S. Grigoleit and G. W. Watson, *Faraday Discuss.*, 2003, **124**, 155–170.
30 S. Kerisit, A. Marmier and S. C. Parker, *J. Phys. Chem. B*, 2005, **109**, 18211–18213.
31 J. P. Perdew, J. A. Chevary, S. H. Vosko, K. A. Jackson, M. R. Pederson, D. J. Singh and C. Fiolhas, *Phys. Rev. B: Condens. Matter*, 1992, **46**, 6671–6687.
32 A. Pavese, M. Catti, S. C. Parker and A. Wall, *Phys. Chem. Miner.*, 1996, **23**.
33 S. C. Parker, E. T. Kelsey, P. M. Oliver and J. O. Titiloye, *Faraday Discuss.*, 1993, **95**, 75–84.
34 S. Hwang, M. Blanco and W. A. Goddard III, *J. Phys. Chem. B*, 2001, **105**, 10746–10752.
35 N. H. de Leeuw and S. C. Parker, *J. Chem. Soc., Faraday Trans.*, 1997, **93**, 467–475.
36 J. O. Titiloye, N. H. de Leeuw and S. C. Parker, *Geochim. Cosmochim. Acta*, 1998, **62**, 2637–2641.
37 N. H. de Leeuw and S. C. Parker, *J. Phys. Chem. B*, 1998, **102**, 2914–2922.
38 D. M. Duffy and J. H. Harding, *Langmuir*, 2004, **20**, 7630–7636.
39 G. Wulff, *Z. Kristallogr. Kristallgeom.*, 1901, **34**, 949.
40 D. Spagnoli, D. J. Cooke, S. Kerisit and S. C. Parker, *J. Mater. Chem.*, 2006, **16**, 1997–2006.
41 P. Curie, *Journal de Physique*, 1894, **3**, 393–415.